European Journal of Nuclear Medicine and Molecular Imaging (2019) 46:776–787
https://doi.org/10.1007/s00259-018-4227-5

ORIGINAL ARTICLE

Comprehensive anatomical and functional imaging in patients with type I neurofibromatosis using simultaneous FDG-PET/MRI

Christian Philipp Reinert[1] · Martin Ulrich Schuhmann[2,3] · Benjamin Bender[4] · Isabel Gugel[2,3] · Christian la Fougère[5] · Jürgen Schäfer[1] · Sergios Gatidis[1]

Received: 10 September 2018 / Accepted: 25 November 2018 / Published online: 8 December 2018

Abstract

Purpose To demonstrate the clinical use of FDG-PET/MRI for monitoring enlargement and metabolism of plexiform neurofibromas (PNF) in patients with neurofibromatosis type 1 (NF1), in whom the development of a malignant peripheral nerve sheath tumor (MPNST) is often a life limiting event.

Methods NF1 patients who underwent a simultaneous FDG-PET/MRI examination in our institution from September 2012 to February 2018 were included. Indication was suspicion of malignant transformation of a PNF to MPNST. A maximum of six peripheral nerve lesions per patient were defined as targets. Standardized uptake values (SUV) and apparent diffusion coefficients (ADC) were measured. The presence of target sign and contrast-medium enhancement was visually recorded. Growth rates were estimated comparing prior or follow-up examinations and correlated with FDG uptake and ADC values. The presence of CNS lesions in cerebral T2 weighted images was recorded.

Results In 28 NF1 patients a total number of 83 peripheral nerve tumors, 75 benign PNFs and eight MPNSTs, were selected as target lesions. The SUVs of MPNSTs were significantly higher than the SUVs of PNF (3.84 ± 3.98 [SUV_{mean} MPNSTs] vs. 1.85 ± 1.03 [SUV_{mean} PNF], $P < .01$). Similarly, lesion SUV_{mean}-to-liver SUV_{mean} ratios significantly differed between MPNSTs and PNF (3.20 ± 2.70 [MPNSTs] vs. 1.23 ± 0.61 [PNF]; $P < .01$). For differentiation between still benign PNF and MPNSTs, we defined $SUV_{max} \geq 2.78$ as a significant cut-off value. Growth rate of PNF correlated significantly positively with SUV_{mean} ($r_s = .41$; $P = .003$). MRI parameters like ADC_{mean} ($1.87 \pm 0.24 \times 10^{-3}$ mm^2/s [PNF] vs. $1.76 \pm 0.11 \times 10^{-3}$ mm^2/s [MPNSTs]; $P > .05$], contrast medium enhancement ($P = .50$) and target sign ($P = .86$) did not differ between groups.

Conclusion Simultaneous FDG-PET/MRI is a comprehensive imaging modality for monitoring PNF in NF1 patients. The combined acquisition of both morphologic information in MRI and metabolic information in PET enables the correlation of lesion growth rates with metabolic activity and to define SUV thresholds of significance to identify malignant transformation, which is of utmost clinical significance.

Keywords PET/MRI · Neurofibromatosis type 1 · Long-term assessment · Malignant peripheral nerve sheath tumor

Introduction

Neurofibromatosis type 1 (NF1) is a neurocutaneous autosomal-dominant genetic disorder caused by a mutation within the tumor suppressor gene NF1 (17q11.2) [1]. Typical manifestations are focal cutaneous or subcutaneous neurofibromas and solitary and plexiform neurofibromas (PNF) of peripheral nerves, which can occur in all parts of

✉ Christian Philipp Reinert
christian.reinert@med.uni-tuebingen.de

[1] Department of Diagnostic and Interventional Radiology, University Hospital Tuebingen, Hoppe-Seyler-Str.3, 72076 Tuebingen, Germany

[2] Department of Neurosurgery, University Hospital Tuebingen, Hoppe-Seyler-Str.3, 72076 Tuebingen, Germany

[3] Centre of Neurofibromatosis, Centre of Rare Diseases, University Hospital Tuebingen, Hoppe-Seyler-Str.3, 72076 Tuebingen, Germany

[4] Department of Diagnostic and Interventional Neuroradiology, University Hospital Tuebingen, Hoppe-Seyler-Str.3, 72076 Tuebingen, Germany

[5] Department of Nuclear Medicine and Clinical Molecular Imaging, University Hospital Tuebingen, Hoppe-Seyler-Str.3, 72076 Tuebingen, Germany

the peripheral nervous systems, beginning in the first, still intradural millimeters, over the intraforaminal and paravertebral part of peripheral nerves to the last distribution in muscles and skin. Physical examination focuses on the NIH criteria based on characteristic features such as cutaneous and nervous neurofibromas, Café au lait macules, osseous dysplasia, optic pathway gliomas, and iris hamartoma (Lisch nodules) [2]. Peripheral nerve neurofibromas appear either as a nodular (solitary) tumor or as diffuse multifocal plexiform neurofibromas (PNF), the latter carrying a significant risk for malignant transformation into malignant peripheral nerve sheath tumors (MPNSTs) with a lifetime risk between 5 and 13% [3, 4]. MPNSTs in NF1 patients which are virtually insensitive to radiation and chemotherapy are the most significant threat to NF1 patients, since they can only be cured by radical resection, which is often only possible at an early stage of disease. Localized MPNSTs may be embedded within parts of more extended PNFs and are, thus, often diagnosed in late stages leading to a poor prognosis [4, 5].

Due to either anatomically difficult to access localizations or involvement of functionally important nerves, surgical resection or (repeated) biopsies of suspicious PNF can be complicated or can carry significant risks [6]. Hence, imaging surveillance plays an important role in NF1 patients. MRI provides a superior soft-tissue contrast compared to CT, allowing a high anatomical resolution. Therefore, MRI is the method-of-choice for anatomical depiction of PNF and for presurgical planning [7]. In addition, MRI is the imaging reference standard for the examination of CNS manifestations of NF1 such as optic nerve gliomas or white matter lesions which are considered to correlate with cognitive dysfunction [8]. Optic gliomas are accompanied by a symptomatic visual loss and carry the risk of malignant transformation into glioblastomas, which are associated with a poor prognosis and poor quality of life [9, 10].

However, malignant transformation of PNF, especially at an early stage, cannot be detected by morphological magnetic resonance imaging (MRI) or computed tomography alone with sufficient accuracy [11]. As increased glucose consumption determined by ^{18}F-FDG-PET has been shown to be a good indicator for malignant transformation of PNF into MPNSTs, ^{18}F-FDG-PET has significantly improved detection and monitoring of malignant lesions in NF1 patients.

Significantly larger tumor sizes of MPNSTs compared to benign solitary parts within PNF have been described, therefore, the interaction between lesion size dynamic and glucose metabolism is of diagnostic importance for monitoring of NF1 patients and needs to be further analyzed [12]. With the introduction of combined PET/MRI all the abovementioned relevant imaging information can be obtained in a single examination [13, 14] thus providing potentially an ideal method for monitoring of patients with NF1.

High cumulative radiation exposure was reported in pediatric patients who receive numerous follow-up PET/CT examinations [15]. Since NF1 is a genetically determined disease with a missing tumor suppressor gene product, the potential risk of induction of malignancy by ionizing radiation is potentially increased compared to other patient cohorts. As the onset of repeated imaging in NF1 patients is mostly in childhood, high radiation exposure should be avoided whenever possible [2]. In addition, the use of PET/MRI instead of PET/CT has been shown to significantly reduce diagnostic radiation exposure in children and adolescents [13].

The purpose of this study was to investigate the clinical use of combined FDG-PET/MRI in patients with NF1 for monitoring enlargement and metabolism of PNFs with regard to malignant transformation, as well as possibility to detect NF1 associated CNS lesions in standard T2 weighted brain images, which are part of the whole body PET/MRI standard protocol.

Methods

Study population

This retrospective study was approved by our local institutional ethical review board and informed consent was waived (Project Number: 345/2018BO).

The underlying study population consisted of all patients with NF1 undergoing FDG-PET/MRI in our institution between September 2012 and February 2018 presenting with a clinical question referring to malignant transformation of known plexiform neurofibromas.

PET/MRI imaging

All combined PET/MRI examinations were performed on an integrated clinical PET/MRI system (Biograph mMR, Siemens Healthcare GmbH, Erlangen, Germany, software versions B20P and E11P) which is able to acquire PET and MRI simultaneously. For the generation of a segmentation-based PET attenuation correction map, a whole-body 3-D T1-weighted spoiled gradient-echo sequence in end-expiratory breath-hold with Dixon-based fat-water separation was acquired. In patients newly examined after January 2017 atlas-based bone-estimation was additionally available and performed for the purpose of attenuation correction. In all PET/MRI examinations the following MR measurements were performed: a transversal and coronal T2-weighted turbo spin echo (TSE) sequence, a coronal whole body short time inversion recovery (STIR) sequence in free breathing, whole body diffusion weighted imaging (DWI), whole body T1-weighted volumetric interpolated breath-hold examination (VIBE) sequence after intravenous injection of 0.1 mmol/kg gadolinium-based MRI contrast media (GADOVIST®), a fluid attenuated inversion recovery

Table 1 Acquisition parameters used in our MRI examination protocol

Variables	T2w axial	T2w coronal	T2 STIR coronal	T1 VIBE post KM	DWI	FLAIR	MPRAGE
Voxel size, mm^3	0.7*0.7*5	1.6*1.6*5	1.8*1.8*5	1.3*1.3*3	1.7*1.7*5	0.78*0.78 (in-plane resolution, mm^2)	0.49*0.49*0.9
Slice thickness, mm	5	5	5	3	5	3	3
B-values, s/mm^2	/	/	/	/	50/800		
Repetition time, ms	1200	1200	6110	3.97	2500	9000	1900
Echo time, ms	96	91	53	1.26	52	87	2.4
Inversion time, ms						2500	900
Bandwidth, Hz/pixel	651	710	300	1040	2442	200	190
Flip angle, degrees	160	160	120	9	90		

(FLAIR) sequence of the head as well as a contrast-enhanced T1-weighted 3-D magnetization prepared rapid gradient echo (MPRAGE) sequence of the head.

Table 1 shows a list of the used MRI sequence parameters.

Patients fasted for at least 6 h before intravenous injection of [^{18}F] fluorodeoxyglucose (FDG). The recommended dose for whole body FDG-PET is weight-dependent and ranges between 3.5–7 MBq/kg for a 2-min scan [16]. As the PET acquisition in PET/MRI is longer (4 min per bed in our case), we reduced these values by a factor of about 2 based on previous data [17]. The injected dose of ^{18}F-FDG patients received was adjusted to patient body weight (average: 2.5 ± 0.60 MBq/kg). The corresponding effective doses of PET in pediatrics and adults were calculated from the applied activity, as described in a previous study [18]. PET acquisition was initiated 60 min after tracer injection.

The whole body scan was acquired over 6 ± 2 bed positions. PET was reconstructed using a 3D ordered-subset expectation-maximization algorithm with 2 iterations, 21 subsets, matrix size 256 × 256, Gaussian filtering of 4 mm. The patient examination times were measured based on the acquisition time stamps that are documented in our Picture Archiving Communication System (PACS) and included an interval of 10 min for repositioning patients in order to achieve whole body coverage, as the scan range was limited to 150 cm until the scanner was updated with an additional scanner coil in 2016.

Quantitative PNF lesion measurements

A maximum of six peripheral nerve target lesions were defined per patient. Of these, a maximum of four nerve target lesions per patient with visibly increased FDG uptake above blood pool levels and a maximum of two target lesions in similar anatomical localization and with similar size without visibly increased FDG uptake were selected. Entirely diffuse configurated plexiform neurofibromas without a definable geometry in MRI, typically infiltrating skin or muscle, were excluded from the evaluation. Image analysis was performed using the software SyngoVia (Siemens, Erlangen, Germany).

Lesion size was determined by measurement of the maximum axial diameter of each target lesion using the T1-weighted MRI sequence after intravenous contrast media application.

For all peripheral nerve lesions, PET quantification was performed measuring the mean, maximum and peak standardized uptake values ($SUV_{mean/max/peak}$) based on 50%-isocontour volumes of interests (VOIs). SUV_{max} is defined as the highest single-pixel value within a defined volume of interest (VOI), whereas SUV_{peak} is defined as an average SUV within a small, fixed-sized VOI (1 ml) centered on the maximum-uptake part of the lesion [19]. For measuring the SUV_{mean} of reference tissues, we placed a 2 cm-diameter ROI in the right atrium (bloodpool) and a 5 cm-diameter ROI in the liver parenchyma. In all patients, lesion SUV_{mean}-to-liver SUV_{mean} ratios were calculated.

In MRI, we measured the mean and minimum apparent diffusion coefficients (ADC_{mean}; ADC_{min}) of all target lesions using circular regions of interest (ROI) with a radius comprising the whole of the lesion on the level of its largest transverse cross-section (large ROI analysis). Additionally, we applied small ROI measurements as previously described [20] in suspicious PNF parts with SUV_{mean} above 2 and MPNSTs by placing a ROI into the lesion area with the highest ^{18}F-FDG-uptake (small ROI analysis).

To assess the long-term development in size of all included PNF lesions, we measured the maximum axial lesion size also in available previous and follow-up PET/MRI or MRI examinations in which the same lesions were assessable (Fig. 1). The growth rate was calculated by the quotient of axial diameter change from previous to follow-up examination and the time interval in months.

Qualitative radiological evaluation

For qualitative analysis, all image data were assessed by two radiologists in consensus. The morphological characteristics of all target lesions were categorized as target-like or not target-like. Target-like lesions were defined as centrally hypointense in T2-weighted images with a hyperintense rim

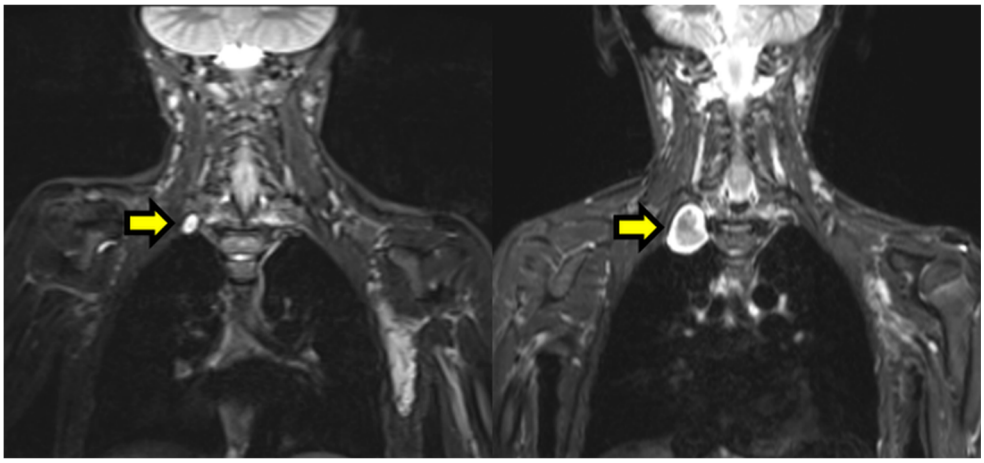

Fig. 1 10-years-old NF1 patient with a PNF lesion in the right upper thoracic aperture in coronal STIR sequence showing significantly increasing size after 3 years of follow-up (left side: MRI only, performed 2013; right side: PET/MRI, performed 2016). In PET/MRI the measured MRI ADC_{mean} of the lesion was 1779 ± 180 × 10^{-3} mm^2/s. The measured PET SUV_{mean} was 2.9 (SUV_{max} 4.2). A MPNST has been proven after surgical resection with subsequent histopathological examination

resembling a target within PNF of peripheral nerves or large PNF accumulations in certain body areas. Contrast-medium enhanced target lesions were defined visually as clearly hyperintense lesions in T1-weighted images after intravenous MRI contrast medium injection.

Furthermore, we evaluated the presence of incidental areas of high signal intensity on T2-weighted FLAIR sequence in the white substance (white matter lesions), which are typical MR findings in the cerebellum, brainstem, basal ganglia and thalami [21]. Also, the presence of visible optic nerve gliomas was evaluated.

Reference standard

All specimens of resected lesions were histologically examined by our in-house pathologists. For non-resected lesions, both the clinical course and imaging follow-up were used as clinical reference standard to characterize the lesion as benign or malignant. The surgical indication was based on a tumor board decision in which all individual cases were discussed.

Statistics

All statistical calculations and graphical illustrations were performed using SPSS Version 22 (IBM Corporation, Armonk, NY). All parameters were tested by the Kolmogorov-Smirnov test for normality. The Kruskal-Wallis test was used for comparing the PET and MRI parameters of benign or malignant target lesions in NF1. The significance level was set at a P value of <.05. Bars with one asterisk mark a level of significance $P < .05$, bars with two asterisks mark a level of significance $P < .01$. The correlation of SUV and neurofibroma growth was assessed by estimating a bivariate correlation and computation of the Spearman's rank correlation coefficient. ROC analysis, including calculation of cut-off values, was performed for differentiation between neurofibromas and MPNSTs.

Results

Study population

Twenty-eight patients [14 female; mean age 20 (2–44) years] with neurofibromatosis type 1 were included. Fifteen patients were children below the age of 18 years.

Of these, 6/28 patients presented with one target lesion, 5/28 patients presented with two target lesions, 8/28 patients presented with three target lesions, 4/28 patients with four target lesions, 3/28 patients with five target lesions and 2/28 patients with six target lesions, respectively.

In the 28 patients cohort, 83 lesions were evaluated, of which 75 were rated as benign target lesions, 53/75 lesions were histologically examined after surgical resection and 22/75 lesions were not resected due to completely stable clinical course and imaging follow-ups (reference standard). In six patients eight histologically proven MPNSTs were found, 5/6 patients had one MPNST and one patient had three MPNSTs.

PET/MRI imaging

There were 23/83 target lesions localized in the extremities, 25/83 target lesions were localized subcutaneously at the abdominal body trunk, intraabdominally or in the pelvis, 25/83 target lesions were localized thoracocervically and 10/83 target lesions were localized paravertebrally. Image examples of a benign target lesion and a MPNST are illustrated in Fig. 2. The mean effective radiation dose patients received in our study was 3.24 ± 1.65 mGy. The estimated mean examination time was 95 ± 21 min per patient including five NF1 patients who had to be repositioned in order to achieve whole body coverage.

Quantitative PNF lesion measurements

The mean size of benign PNF lesions was 2.65 ± 1.83 cm, whereas the mean size of MPNSTs was 3.54 ± 1.11 cm ($P < .01$).

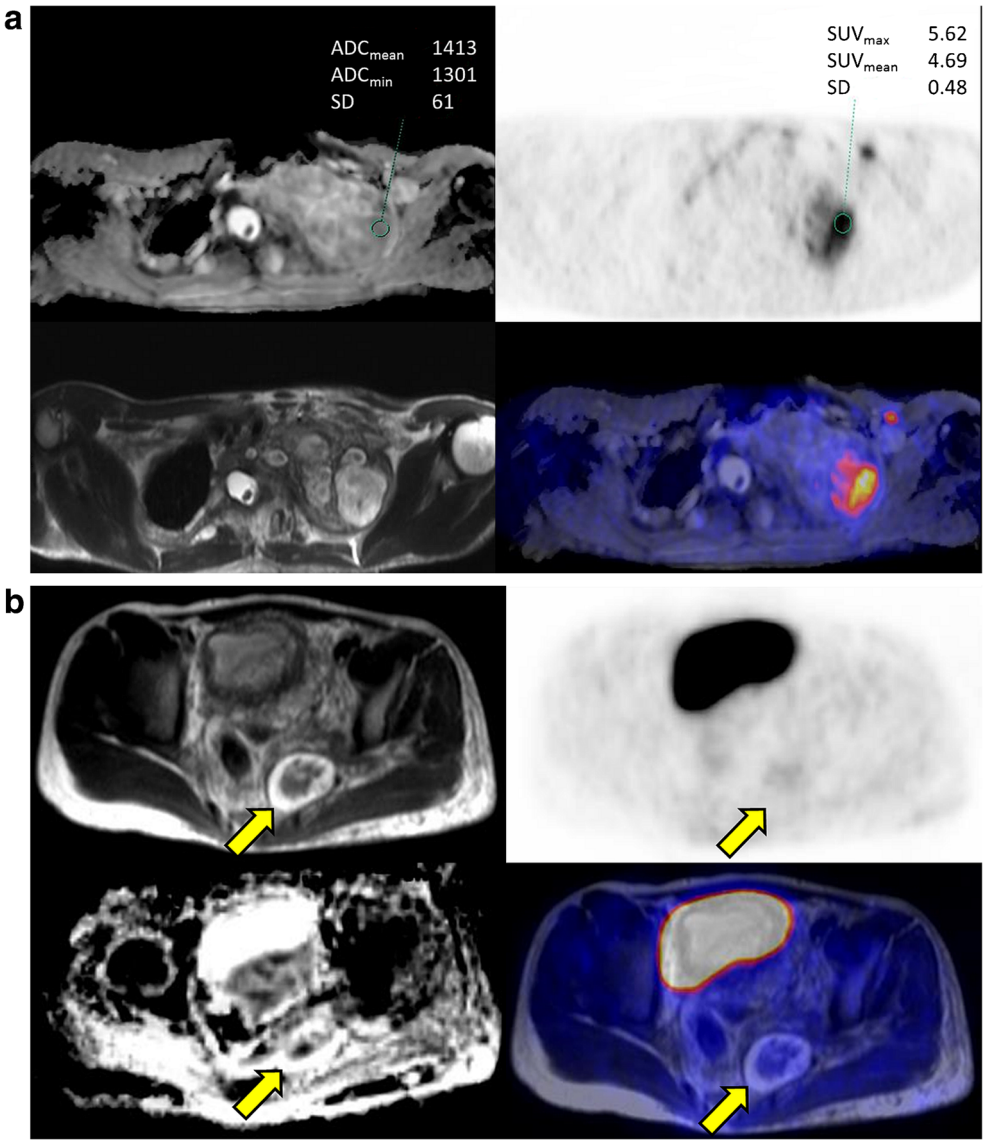

Fig. 2 **a** 28-years-old NF1 patient with a MPNST in the left upper thoracic aperture located within a large PNF manifestation showing a heterogeneous diffusion restriction in ADC map (first row, left side). A small ROI was placed in the area with the most increased glucose metabolism in FDG-PET (first row, right side), copied and pasted in the ADC map for measurement. The second row on the left side shows the lesion in T2-weighted axial sequence. **b** 10-years-old NF1 patient with a benign PNF lesions in the left ischiorectal fossa showing a target-like configuration in T2-weighted axial sequences (fourth row, left side), a heterogeneous diffusion restriction in ADC map (third row, left side) and a glucose metabolism in FDG-PET below bloodpool SUV (third/fourth row, right side)

The measured PET SUV_{mean} of histologically proven MPNSTs was significantly higher than the SUV_{mean} of benign PNF lesions (3.84 ± 3.98 [MPNSTs] vs. 1.85 ± 1.03 [PNF]; $P < .01$) (Fig. 3a). The SUV_{max} of histologically proven MPNSTs was similarly higher than the SUV_{max} of benign PNF (5.84 ± 6.10 [MPNSTs] vs. 3.03 ± 1.92 [PNF]; $P < .01$) (Fig.3b). Similarly, the lesion SUV_{mean}-to-liver SUV_{mean} ratio significantly differed between MPNSTs and PNF lesions (3.20 ± 2.70 [MPNSTs] vs. 1.23 ± 0.61 [PNF]; $P < .01$) (Fig. 4). As significant cut-off values for differentiation between still benign PNF and MPNSTs, we calculated $SUV_{max} \geq 2.78$ (sensitivity 0.88; specificity 0.73) and 1.45 for lesion SUVmean-to-liver SUVmean ratio (sensitivity 0.88; specificity 0.79).

MPNSTs showed only a tendency for higher diffusion restriction in large ROI analysis, which, however, did not reach statistical significance (ADC_{mean} values of benign PNF lesions and MPNSTs ($1.87 \pm 0.24 \times 10^{-3}$ mm^2/s [PNF] vs. $1.76 \pm 0.11 \times 10^{-3}$ mm^2/s [MPNSTs]; $P = 1.0$]. (Fig. 5a). Similarly, small ROI analysis in lesion areas with the highest ^{18}F-FDG-uptake showed a tendency towards lower $ADC_{mean/min}$ values in MPNSTs compared to benign PNF with $SUV_{mean} > 2$ without statistical significance ($P > .05$) (Fig. 5b).

There were 24/28 patients that had both a previous (mean time interval: 21.63 ± 13.38 months) and follow-up (mean time interval: 13.26 ± 7.94 months) PET/MRI or MRI examination. The estimated lesion growth rate correlated significantly with an increased glucose consumption as measured by means of PET SUV_{mean} ($r_s = .41$; $P = .003$) (Fig. 6a), whereas no significant correlation was found between the lesion growth rate and the MRI ACD_{mean} in large ROI analysis ($r_s = .07$; $P = .67$) (Fig. 6b).

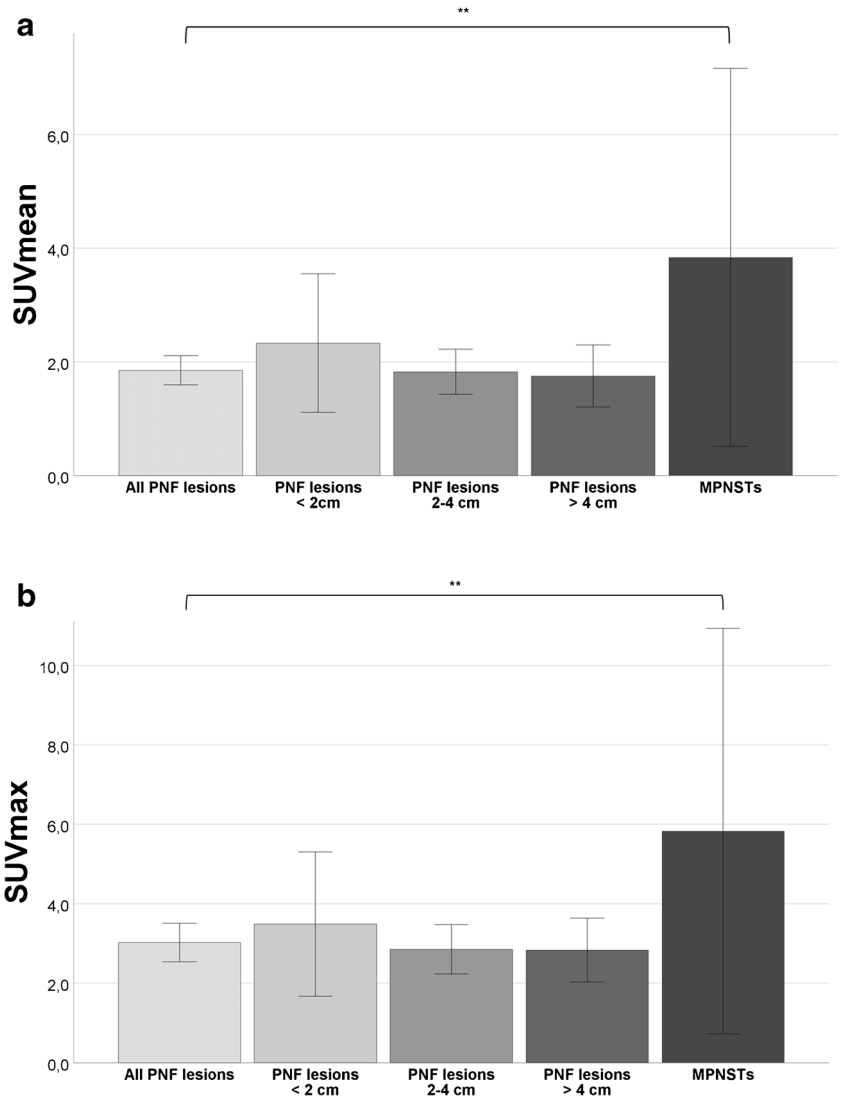

Fig. 3 **a** $SUV_{mean} \pm 95\%$ CI of all benign PNF lesions ($n = 75$), lesions <2 cm in diameter ($n = 21$), lesions 2–4 cm in diameter ($n = 30$), lesions >4 cm in diameter ($n = 16$) and MPNSTs ($n = 8$). **b** $SUV_{max} \pm 95\%$ CI of all benign PNF lesions ($n = 75$), lesions <2 cm in diameter ($n = 21$), lesions 2–4 cm in diameter ($n = 30$), lesions >4 cm in diameter ($n = 16$) and MPNSTs ($n = 8$)

25/75 benign PNF lesions presenting with a SUV_{mean} value below that of bloodpool SUV_{mean} (0.95 ± 0.30) showed a significant lower growth rate per month than 50/75 benign PNF lesions with a relatively elevated SUV_{mean} value (−0.32

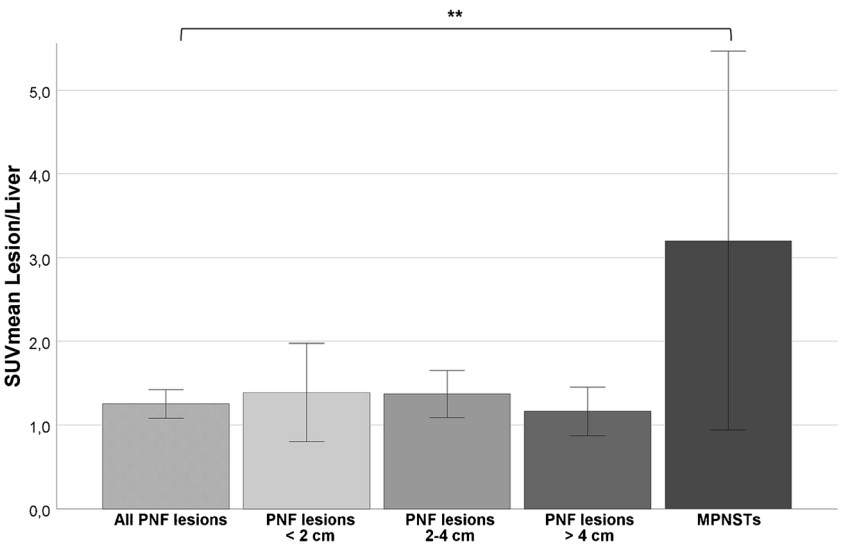

Fig. 4 Lesion SUV_{mean}-to-liver SUV_{mean} ratio $\pm 95\%$ CI of all benign PNF lesions ($n = 75$), lesions <2 cm in diameter ($n = 21$), lesions 2–4 cm in diameter ($n = 30$), lesions >4 cm in diameter ($n = 16$) and MPNSTs ($n = 8$)

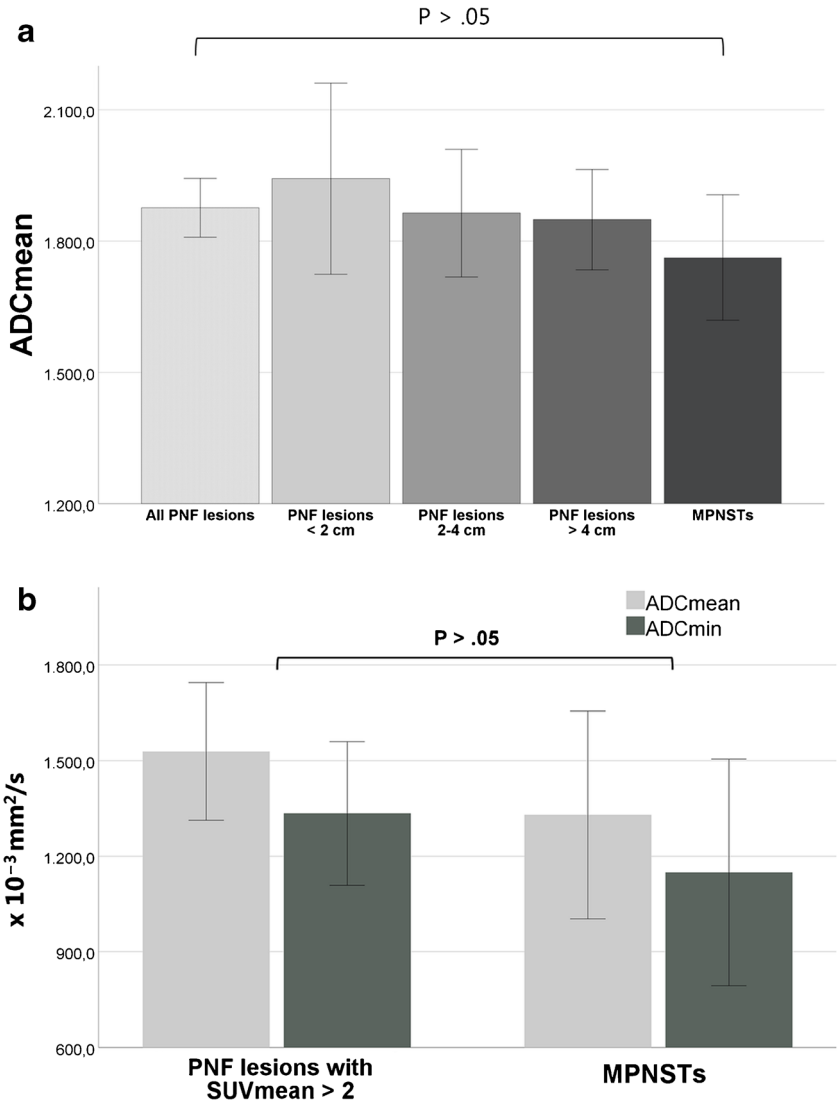

Fig. 5 **a** ADC_{mean} ± 95% CI using large ROI analysis of all benign PNF lesions ($n = 75$), lesions <2 cm in diameter ($n = 21$), lesions 2–4 cm in diameter ($n = 30$), lesions >4 cm in diameter ($n = 16$) and MPNSTs ($n = 8$). **b** ADC_{mean} and ADC_{min} ± 95% CI using small ROI analysis of lesions with a measured SUVmean >2 ($n = 13$) and MPNSTs ($n = 8$)

± 1.00%/month [SUVmean < bloodpool] vs. 1.10 ± 2.25%/month [SUVmean > bloodpool]; $P < .05$) (Fig. 7).

Qualitative radiological evaluation

There were 49/75 benign PNF lesions and 6/8 MPNSTs that showed an enhancement of contrast media, whereas 26/75 benign PNF lesions did not enhance ($P = .50$). Also, 35/75 benign PNF lesions and 4/8 MPNSTs had a positive target sign ($P = .86$).

In addition, 8/28 patients did not get an examination of the brain in PET/MRI because of an inconspicuous brain MRI examination performed shortly before the PET/MRI scan. The PET/MRI of 20/28 patients included a dedicated T2 weighted FLAIR brain protocol for screening purposes as described above. Out of these 20 patients, 14 patients (70%) had T2-hyperintense focal areas of signal intensity (FASI) in brain parenchyma. Furthermore, we found changes compatible with optic nerve gliomas in eight patients (40%) (Fig. 8).

Discussion

In this study, we investigated the clinical usability of combined FDG-PET/MRI imaging in patients with neurofibromatosis type 1. PET/MRI provides the unique possibility to unite the advantages of high sensitive MRI, namely the superior soft-tissue contrast compared to CT, the ability to acquire information about cellular density with diffusion weighted imaging and the possibility of multiparametric tissue characterization by acquisition of complementary metabolic information in PET. The combination of these two image modalities in one examination simplifies the clinical workflow and reduces both the number of necessary sedations in younger children and, compared to PET/CT, the radiation exposure, which is most important in a disease that is characterized by a loss of a tumor suppression gene product and where many children and adolescents need to be investigated.

MPNSTs showed significant higher glucose metabolic activity than benign PNF lesions in PET and tend to have a higher diffusion restriction in diffusion weighted MRI as a sign of

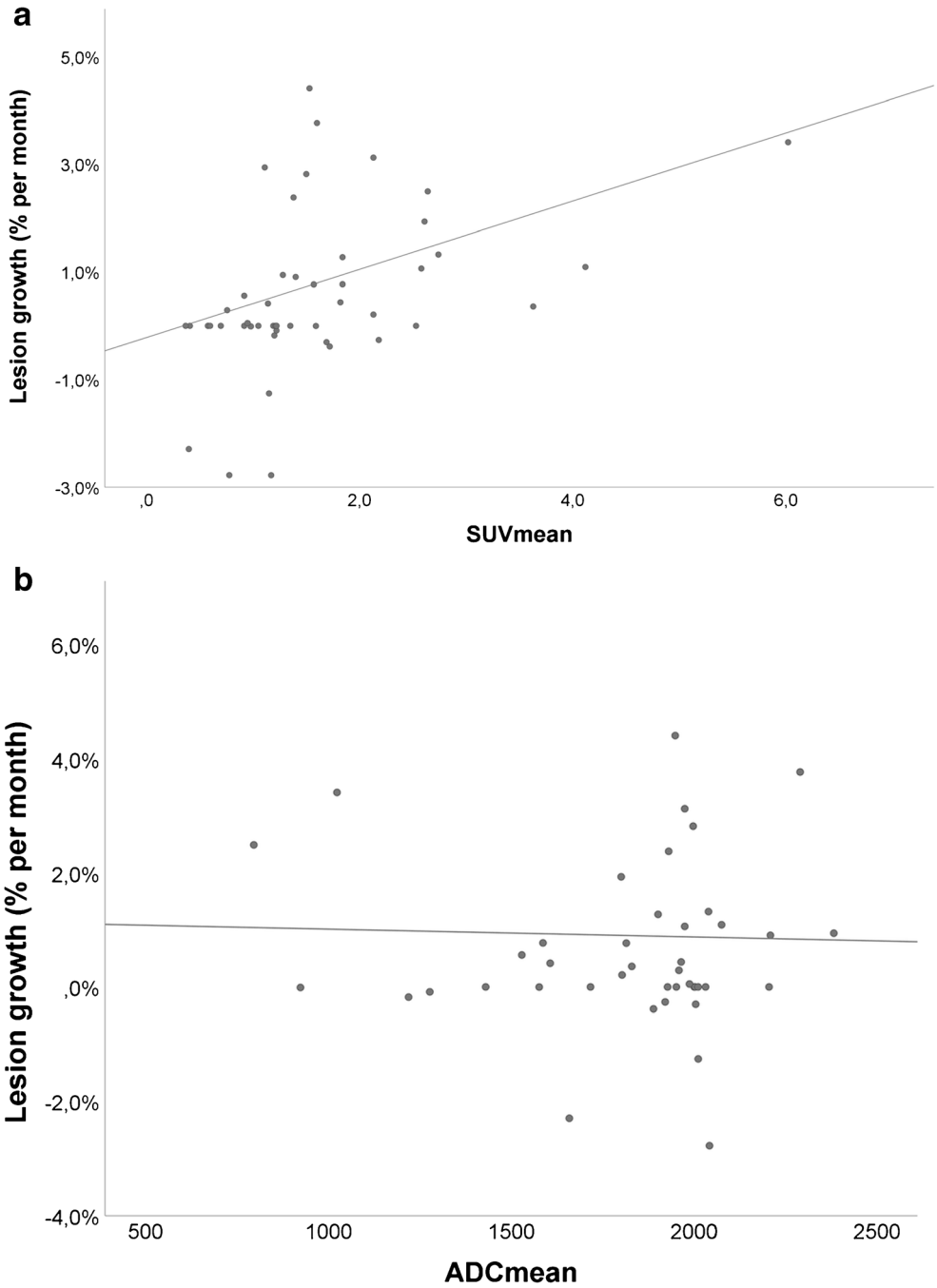

Fig. 6 **a** Bivariate correlation curve between the SUV_{mean} and the lesion growth rate (percent per month) with a calculated Spearman's rank correlation coefficient $r_s = .4$ and a *P* value of .003. **b** Bivariate correlation curve between the ADC_{mean} using large ROI analysis and the lesions growth (percent per month) with a calculated Spearman's rank correlation coefficient $r_s = .07$ and a *P* value of .67

increased cellularity. No differences between MPNSTs and benign PNF lesions were observed in lesion morphology or contrast behavior.

These results are in concordance with previous studies showing that MPNSTs have an increased consumption of ^{18}F-FDG compared to benign PNF lesions in NF1 patients [5, 22–24]. However, the predictive performance of PET SUV for non-invasive detection and characterization of MPNSTs is still under debate. Our calculated cut-off SUV_{max} (2.78) has a sensitivity of 88% and a specificity of 73%, which is in the range of the published heterogeneous range of SUV_{max} cut-off values from 1.5 to 6.1 to distinguish between MPNSTs and benign PNF lesions [25, 26]. Nevertheless, a $SUV_{max} \geq 3.5$ has been widely used in the literature as a cut-off for malignant transformation into MPNSTs [5, 25, 27–31].

Due to technical and physiological factors, PET quantification with SUV measurements has a limited reliability [32, 33], therefore, an interinstitutional standardization in SUV quantification is advisable. To improve reproducibility of quantitative SUV measurement, the use of lesion-to-liver ratios has been recommended as a semi-quantitative index [5, 11]. Therefore, several authors have performed semi-quantitative analyses measuring the FDG-

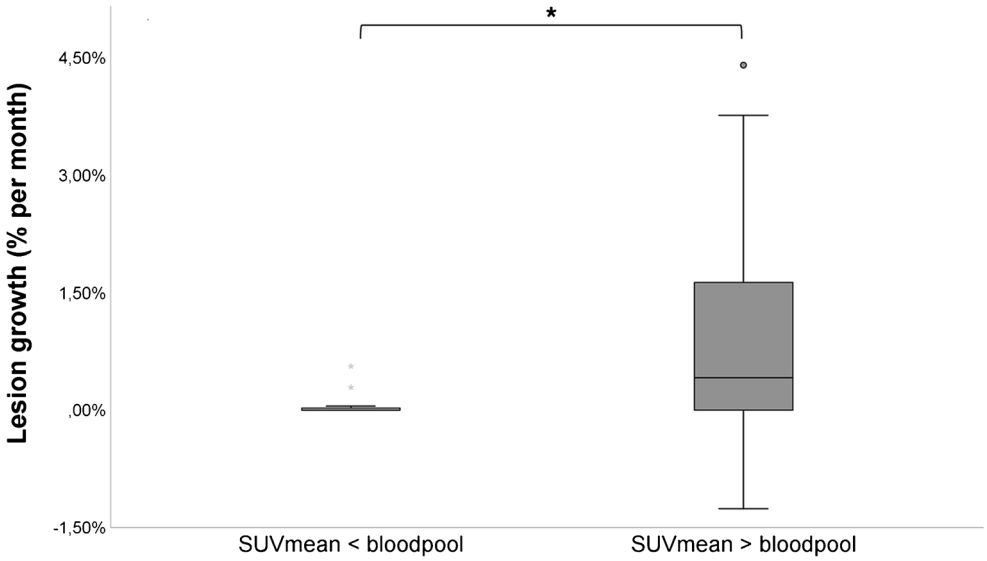

Fig. 7 Growth rate (percent per month) ± 95% CI in benign PNF lesions with a measured SUV_{mean} < bloodpool ($n = 25$) and in benign PNF lesions with a measured SUV_{mean} > bloodpool ($n = 50$)

uptake in the liver as the most used reference tissue [34]. In our study, we calculated lesion SUV_{mean}-to-liver SUV_{mean} ratios using a cut-off value of 1.45 to distinguish between benign PNF lesions and MPNSTs with a sensitivity of 0.88 and a specificity of 0.79. This was our threshold parameter with the highest discriminatory power, which is slightly lower than in a study of Combemale et al. [35]. However, Combemale et al. used the SUV_{max} values of the measured lesions and liver.

Interestingly, lesion growth rate of benign PNF lesions correlated significantly positively with an increased glucose metabolism. Thus, quantitative analysis of FDG-uptake as a marker of cell glucose metabolism allows not only to differentiate between benign PNF lesions and MPNSTs but also to characterize lesions carrying an increased risk of malignancy. As CT-based volume measurements do not provide information about lesion viability, we therefore advocate the monitoring of both size development and metabolic changes in benign PNF lesions. A further improvement of the correlation between growth rate and metabolic activity might be possible if benign PNF lesions are assessed by volumetric analysis, which is, however, technically, and regarding time efforts, more demanding in clinical routine than simple assessment of the largest axial diameter of a lesion.

In DWI, MPNSTs showed a tendency for lower ADC values using large ROI analysis, however, this result was not statistically significant in our cohort. A tendency for lower ADC values in MPNSTs was also observed using small ROIs in lesion areas with the highest ^{18}F-FDG-uptake. Our results are consistent with previous studies showing overlapping ADC values for soft tissue benign and malignant tumors [36, 37]. As a marker of tumor cellularity due to restricted diffusion of water in regions of high cellularity, the use of quantitative DWI has been reported for distinguishing benign and malignant soft tissue tumors [38].

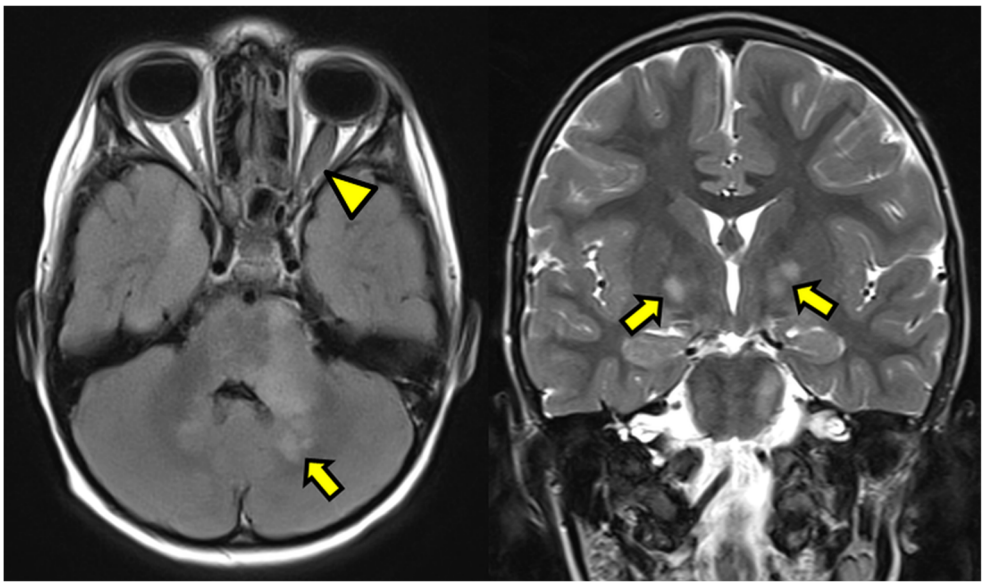

Fig. 8 Axial FLAIR-sequence (left side) and coronal T2-weighted TSE sequence of a 10-years-old NF1 patient with multiple T2-hyperintense focal areas of signal intensity (FASI) in the thalamic region of the brain (arrows) and a glioma of the left optic nerve (arrowhead)

Thus, DWI may be a potentially useful marker for monitoring PNF development in NF1 patients in a larger study cohort. However, DWI might be affected not only by cellularity alone but also by the nature of the extracellular matrix. Both benign PNF lesions and MPNSTs characteristically contain myxoid extracellular matrix in varying extent [39, 40]. Myxoid tissue has a gelatinous stroma with high levels of hyaluronic acid and immature collagen fibers leading to abundant free water molecules in extracellular spaces [7]. Atypical neurofibromas with variable pathologic features containing degenerative cytological atypia or increased cellularity, as well as "hybrid" nerve sheath tumors showing histologic features of both neurofibromas and schwannomas have been described [41, 42]. As MPNSTs are most often embedded within preexisting plexiform neurofibromas, the tumor tissue within a chosen ROI for ADC analysis may contain both benign and malignant fractions [30].

The previously reported target sign as a morphological feature of malignancy and contrast enhancement behaviour did not significantly differ between benign and malignant lesions. Several other studies reported the target sign as a useful diagnostic sign of MPNSTs compared to benign plexiform neurofibromas [23, 43, 44]. Our study did not support this observation and is in concordance with a study of Demehri et al. showing no significant difference in the presence of a target sign comparing neurofibromas and MPNSTs [12]. As a hyperintense peripheral zone on T2-weighted sequences reflects nonfibrillary myxomatous tissue and a hypointense central zone reflects dense collagen, the abovementioned heterogeneity of both myxoid extracellular matrix and cellularity may result in more or less uniform signal characteristics [42, 45]. Intratumoral necrotic or less well perfused areas within faster growing still benign PNF lesions or MPNSTs may be an explanation for heterogeneous contrast enhancement [30].

As further morphologic characteristics of MPNSTs, an irregular tumor shape, unclear margin and intratumoral lobulation were described while still benign PNF lesions were described as homogeneous isointense to skeletal muscle on T1-weighted sequences, heterogeneous hyperintense on fluid-sensitive sequences and heterogeneous contrast enhancing [44, 46]. Our study cohort included patients that were closely monitored due to the underlying disease neurofibromatosis type 1. In these patients, the histologically proven MPNSTs were detected in early stages without infiltration of surrounding tissue. Therefore, in our qualitative analysis, we focused on previously described MRI features for peripheral lesions, target sign and contrast medium enhancement, and their potential change if malignant transformation into MPNSTs occurs. Further MRI imaging features including "perilesional edema", "necrosis" and "irregular margins" can be mainly observed in advanced stage MPNSTs with infiltration of surrounding tissue and were, thus, not observed in our patient cohort. Nevertheless, no general MRI-derived parameters have yet been accepted as criteria for distinguishing MPNSTs from still benign PNF lesions because none of these imaging features allowed a clear differentiation [23].

Cerebral FASI were detected in 70% of our NF1 patient cohort whereas 40% had optic nerve gliomas, resembling observations of other studies [47]. These findings point out that a whole body PET/MRI also provides clinically relevant screening information about the brain in only one examination. Certainly one cerebral FLAIR sequence is not sufficient to assess any brain lesion, therefore, we recommend that suspicious changes in such a sequence have to be prompted by a dedicated diagnostic MRI of the brain including contrast administration to reliably evaluate any intracranial changes.

In our study patients received a mean effective radiation dose of 3.24 ± 1.65 mGy, which is significantly lower compared to the radiation exposure patients normally receive in whole-body PET/CT scans with CT accounting for the larger part of the total effective dose [13, 17]. By extending PET acquisition time per bed position compared to PET/CT, a reduction in administered tracer activity was already possible in PET/MRI. Further technical developments, for example the use of newly introduced Silicon-Photomultiplier Detectors (SiPM), which are not part of the used PET/MRI scanner, can potentially further reduce radiation exposure to patients [48]. Whole body PET/MRI examinations are associated with long examination times exceeding 1 h, similar to whole body MRI. The additional PET scan does not significantly increase examination times as it is performed simultaneously. In the near future the use of advanced MRI acceleration techniques, such as simultaneous multi-slice (SMS) DWI and compressed sensing methods will likely result in marked reduction of examination times [49, 50].

This study has limitations. All included patients in our study had peripheral nerve lesions due to genetically proven NF1. Hence, our study cannot answer the question how sporadic MPNSTs differ compared to MPNSTs in NF1 patients in terms of lesion characteristics. As NF1-asssociated MPNSTs are mostly embedded within preexisting plexiform neurofibromas, this could be a characteristic to differentiate them from de novo arising MPNSTs. Further, NF1-associated MPNSTs are associated with a worse survival outcome compared to sporadic MPNSTs [51] and could thus be linked with a greater extent of intratumoral necrotic areas or less well perfused areas due to faster growing. Another important point is that NF1-associated MPNSTs typically show a higher incidence of multifocal nature [52].

From a technical point of view, PET quantification of paravertebral PNF lesions may have reduced accuracy due to the known error of MR-based attenuation correction in this localization. However, this shortcoming can be overcome by using atlas-based methods for PET/MRI attenuation correction as implemented in our cohort in more recent examinations [53]. The size of our study cohort is limited. Further prospective studies with a larger group of patients are necessary in order to obtain more detailed insight into the rare disease of NF1.

Conclusions

Simultaneous PET/MRI is a comprehensive imaging modality for monitoring PNF in NF1 patients. The combined acquisition of both morphologic information in MRI and metabolic information in PET enables the correlation of lesion growth rates with metabolic activity and to define SUV thresholds of significance to identify malignant transformation, which is of utmost clinical significance.

Compliance with ethical standards

Conflict of interest Benjamin Bender received travel support by Bayer Vital and consultancy fees from Medtronic.

Ethical approval All procedures performed in studies involving human participants were in accordance with the ethical standards of the institutional and/or national research committee and with the 1964 Helsinki Declaration and its later amendments or comparable ethical standards.

This retrospective study was approved by our local institutional ethical review board and informed consent was waived (Project Number: 345/2018BO).

References

1. Yap YS, et al. The NF1 gene revisited - from bench to bedside. Oncotarget. 2014;5(15):5873–92.
2. Ferner RE, et al. Guidelines for the diagnosis and management of individuals with neurofibromatosis 1. J Med Genet. 2007;44(2):81–8.
3. Ducatman BS, et al. Malignant peripheral nerve sheath tumors. A clinicopathologic study of 120 cases. Cancer. 1986;57(10):2006–21.
4. Evans DG, et al. Malignant peripheral nerve sheath tumours in neurofibromatosis 1. J Med Genet. 2002;39(5):311–4.
5. Combemale P, et al. Utility of 18F-FDG PET with a semi-quantitative index in the detection of sarcomatous transformation in patients with neurofibromatosis type 1. PLoS One. 2014;9(2):e85954.
6. Canavese F, Krajbich JI. Resection of plexiform neurofibromas in children with neurofibromatosis type 1. J Pediatr Orthop. 2011;31(3):303–11.
7. Wu JS, Hochman MG. Soft-tissue tumors and tumorlike lesions: a systematic imaging approach. Radiology. 2009;253(2):297–316.
8. Piscitelli O, et al. Neurofibromatosis type 1 and cerebellar T2-hyperintensities: the relationship to cognitive functioning. Dev Med Child Neurol. 2012;54(1):49–51.
9. Gayre GS, et al. Long-term visual outcome in patients with anterior visual pathway gliomas. J Neuroophthalmol. 2001;21(1):1–7.
10. Omuro A, DeAngelis LM. Glioblastoma and other malignant gliomas: a clinical review. JAMA. 2013;310(17):1842–50.
11. Broski SM, et al. Evaluation of 18F-FDG PET and MRI in differentiating benign and malignant peripheral nerve sheath tumors. Skelet Radiol. 2016;45(8):1097–105.
12. Demehri S, et al. Conventional and functional MR imaging of peripheral nerve sheath tumors: initial experience. AJNR Am J Neuroradiol. 2014;35(8):1615–20.
13. Gatidis S, et al. Comprehensive oncologic imaging in infants and preschool children with substantially reduced radiation exposure using combined simultaneous (1)(8)F-Fluorodeoxyglucose positron emission tomography/magnetic resonance imaging: a direct comparison to (1)(8)F-Fluorodeoxyglucose positron emission tomography/computed tomography. Investig Radiol. 2016;51(1):7–14.
14. Lu-Emerson C, Plotkin SR. The neurofibromatoses. Part 1: NF1. Rev Neurol Dis. 2009;6(2):E47–53.
15. Chawla SC, et al. Estimated cumulative radiation dose from PET/CT in children with malignancies: a 5-year retrospective review. Pediatr Radiol. 2010;40(5):681–6.
16. Boellaard R, et al. FDG PET/CT: EANM procedure guidelines for tumour imaging: version 2.0. Eur J Nucl Med Mol Imaging. 2015;42(2):328–54.
17. Schafer JF, et al. Simultaneous whole-body PET/MR imaging in comparison to PET/CT in pediatric oncology: initial results. Radiology. 2014;273(1):220–31.
18. Radiation dose to patients from radiopharmaceuticals (addendum 2 to ICRP publication 53). Ann ICRP. 1998;28(3):1–126. http://www.icrp.org/publication.asp?id=ICRP%20Publication%2080. Accessed 30 Nov 2018.
19. Vanderhoek M, Perlman SB, Jeraj R. Impact of the definition of peak standardized uptake value on quantification of treatment response. J Nucl Med. 2012;53(1):4–11.
20. Neubauer H, et al. Diagnostic value of diffusion-weighted MRI for tumor characterization, differentiation and monitoring in pediatric patients with neuroblastic tumors. Rofo. 2017;189(7):640–50.
21. Billiet T, et al. Characterizing the microstructural basis of "unidentified bright objects" in neurofibromatosis type 1: a combined in vivo multicomponent T2 relaxation and multi-shell diffusion MRI analysis. Neuroimage Clin. 2014;4:649–58.
22. Salamon J, et al. 18F-FDG PET/CT for detection of malignant peripheral nerve sheath tumours in neurofibromatosis type 1: tumour-to-liver ratio is superior to an SUVmax cut-off. Eur Radiol. 2014;24(2):405–12.
23. Derlin T, et al. Comparative effectiveness of 18F-FDG PET/CT versus whole-body MRI for detection of malignant peripheral nerve sheath tumors in neurofibromatosis type 1. Clin Nucl Med. 2013;38(1):e19–25.
24. Van Der Gucht A, et al. Metabolic tumour burden measured by 18F-FDG PET/CT predicts malignant transformation in patients with Neurofibromatosis Type-1. PLoS One. 2016;11(3):e0151809.
25. Warbey VS, et al. [18F]FDG PET/CT in the diagnosis of malignant peripheral nerve sheath tumours in neurofibromatosis type-1. Eur J Nucl Med Mol Imaging. 2009;36(5):751–7.
26. Bredella MA, et al. Value of PET in the assessment of patients with neurofibromatosis type 1. AJR Am J Roentgenol. 2007;189(4):928–35.
27. Ferner RE, et al. [18F]2-fluoro-2-deoxy-D-glucose positron emission tomography (FDG PET) as a diagnostic tool for neurofibromatosis 1 (NF1) associated malignant peripheral nerve sheath tumours (MPNSTs): a long-term clinical study. Ann Oncol. 2008;19(2):390–4.
28. Ferner RE, et al. Evaluation of (18)fluorodeoxyglucose positron emission tomography ((18)FDG PET) in the detection of malignant peripheral nerve sheath tumours arising from within plexiform neurofibromas in neurofibromatosis 1. J Neurol Neurosurg Psychiatry. 2000;68(3):353–7.
29. Chirindel A, et al. 18F-FDG PET/CT qualitative and quantitative evaluation in neurofibromatosis type 1 patients for detection of malignant transformation: comparison of early to delayed imaging with and without liver activity normalization. J Nucl Med. 2015;56(3):379–85.
30. Benz MR, et al. Utilization of positron emission tomography in the management of patients with sarcoma. Curr Opin Oncol. 2009;21(4):345–51.

31. Benz MR, et al. Quantitative F18-fluorodeoxyglucose positron emission tomography accurately characterizes peripheral nerve sheath tumors as malignant or benign. Cancer. 2010;116(2):451–8.
32. Kumar V, et al. Variance of SUVs for FDG-PET/CT is greater in clinical practice than under ideal study settings. Clin Nucl Med. 2013;38(3):175–82.
33. de Langen AJ, et al. Repeatability of 18F-FDG uptake measurements in tumors: a metaanalysis. J Nucl Med. 2012;53(5):701–8.
34. Laffon E, et al. Is liver SUV stable over time in (1)(8)F-FDG PET imaging? J Nucl Med Technol. 2011;39(4):258–63.
35. Combemale P, et al. Utility of 18F-FDG PET with a semi-quantitative index in the detection of sarcomatous transformation in patients with neurofibromatosis type 1. PLoS One. 2014. 9(2): e85954.
36. Nagata S, et al. Diffusion-weighted imaging of soft tissue tumors: usefulness of the apparent diffusion coefficient for differential diagnosis. Radiat Med. 2008;26(5):287–95.
37. Einarsdóttir H, et al. Diffusion-weighted MRI of soft tissue tumours. Eur Radiol. 2004;14(6):959–63.
38. Razek A, et al. Assessment of soft tissue tumours of the extremities with diffusion echoplanar MR imaging. Radiol Med. 2012;117(1): 96–101.
39. Masayuki M, et al. Soft-tissue tumors evaluated by line-scan diffusion-weighted imaging: influence of myxoid matrix on the apparent diffusion coefficient. J Magn Reson Imaging. 2007;25(6):1199–204.
40. Petscavage-Thomas JM, et al. Soft-tissue myxomatous lesions: review of salient imaging features with pathologic comparison. Radiographics. 2014;34(4):964–80.
41. Rodriguez FJ, et al. Pathology of peripheral nerve sheath tumors: diagnostic overview and update on selected diagnostic problems. Acta Neuropathol. 2012;123(3):295–319.
42. Feany MB, Anthony DC, Fletcher CD. Nerve sheath tumours with hybrid features of neurofibroma and schwannoma: a conceptual challenge. Histopathology. 1998;32(5):405–10.
43. Matsumine A, et al. Differentiation between neurofibromas and malignant peripheral nerve sheath tumors in neurofibromatosis 1 evaluated by MRI. J Cancer Res Clin Oncol. 2009;135(7):891–900.
44. Bhargava R, et al. MR imaging differentiation of benign and malignant peripheral nerve sheath tumors: use of the target sign. Pediatr Radiol. 1997;27(2):124–9.
45. Suh JS, et al. Peripheral (extracranial) nerve tumors: correlation of MR imaging and histologic findings. Radiology. 1992;183(2):341–6.
46. Lin J, Martel W. Cross-sectional imaging of peripheral nerve sheath tumors: characteristic signs on CT, MR imaging, and sonography. AJR Am J Roentgenol. 2001;176(1):75–82.
47. Sevick RJ, et al. Evolution of white matter lesions in neurofibromatosis type 1: MR findings. AJR Am J Roentgenol. 1992;159(1): 171–5.
48. Sekine T, et al. Reduction of (18)F-FDG dose in clinical PET/MR imaging by using silicon photomultiplier detectors. Radiology. 2018;286(1):249–59.
49. Taron J, et al. Simultaneous multislice diffusion-weighted imaging in whole-body positron emission tomography/magnetic resonance imaging for multiparametric examination in oncological patients. Eur Radiol. 2018;28(8):3372–83.
50. Kustner T, et al. Self-navigated 4D cartesian imaging of periodic motion in the body trunk using partial k-space compressed sensing. Magn Reson Med. 2017;78(2):632–44.
51. Watson KL, et al. Patterns of recurrence and survival in sporadic, neurofibromatosis type 1-associated, and radiation-associated malignant peripheral nerve sheath tumors. J Neurosurg. 2017;126(1): 319–29.
52. Kar M, et al. Malignant peripheral nerve sheath tumors (MPNST)–clinicopathological study and treatment outcome of twenty-four cases. World J Surg Oncol. 2006;4:55.
53. Sekine T, et al. Evaluation of atlas-based attenuation correction for integrated PET/MR in human brain: application of a head atlas and comparison to true CT-based attenuation correction. J Nucl Med. 2016;57(2):215–20.